Acta Geodyn. Geomater., Vol. 22, No. 2 (218), 183–194, 2025
DOI: 10.13168/AGG.2025.0012

journal homepage: https://www.irsm.cas.cz/acta

ORIGINAL PAPER

OBSERVING-SESSION DURATION OPTIMIZATION OF GPS DEFORMATION NETWORKS USING POINT-SENSITIVITY ELLIPSES

Muharrem Hilmi ERKOÇ *, Uğur DOĞAN and Cüneyt AYDIN

Yildiz Technical University, Department of Geomatic Engineering, 34220 Istanbul, Türkiye

**Corresponding author's e-mail:* mherkoc@yildiz.edu.tr

ARTICLE INFO

Article history:
Received 27 February 2025
Accepted 22 April 2025
Available online 29 April 2025

Keywords:
GPS
Observing session duration
Sensitivity,
Displacement
Non-centrality parameters

ABSTRACT

This study investigates the relationship between GPS observing session duration and sensitivity, measured using non-centrality parameters. TUSAGA-AKTIF (Türkiye's CORS-TR) network with 15 stations was used for this aim. Data with 4h, 6h, 12h, and 24h observing session durations from three sequential days in 2011, 2012, and 2013 were analyzed using Bernese 5.2 GPS software. The repeatability of the daily solutions for each year was carefully analyzed to properly scale the Bernese cofactor matrices. The root mean square (RMS) values for daily repeatability relative to the combined 3-day solution were computed (generally less than 2 mm in horizontal directions (north and east for 24h observing sessions).

For each yearly dataset, a comparison of non-centrality parameters revealed a linear relationship between session duration and non-centrality parameters. Using the cofactor matrices obtained from these observing sessions, the minimum detectable displacements along the maximum eigen directions were compared. Results showed that longer session durations led to smaller minimum detectable displacements, establishing a linear relationship between observing session duration and minimum detectable displacement. Finally, sensitivity ellipses were drawn using the minimum detectable displacement parameters.

INTRODUCTION

The sensitivity of a deformation monitoring network refers to its ability to detect and measure positional changes within a given area. Alongside accuracy and reliability, sensitivity is a key criterion in network optimization, as it determines the smallest displacements that can be reliably identified (Alizadeh -Khameneh et al., 2015). Sensitivity analysis specifically reveals the minimum displacement detectable in monitoring networks, thus providing essential information about network quality.

In designing monitoring networks, the possible deformation model can be predicted using prior information derived from geological, seismic, and geodetic surveys (Even-Tzur, 1999). This a priori information plays a vital role in regional monitoring networks by preventing unmodeled systematic effects from affecting coordinate estimates and leading to incorrect deformation conclusions (Betti et al., 1999). Therefore, monitoring networks must be designed to detect displacements or deformation parameters with specified probabilities α and β (α being the level of significance, β being test power) (Koch, 1988; Kuang, 1991; Betti et al., 1999; Even-Tzur, 1999).

Recent studies have significantly advanced our understanding of GPS sensitivity in deformation monitoring. Wang et al. (2021) demonstrated the crucial role of observation duration in structural health monitoring applications, while Forootan et al. (2021) enhanced displacement prediction reliability using Kalman filtering-based time series analysis. These findings complement earlier work by Xu and Grafarend (1995), who introduced multi-objective optimal design for deformation networks, and Even-Tzur (2002), who designed GPS vector configurations based on baseline contributions to network sensitivity. Additionally, Martin et al.'s (2015) study further emphasizes the potential of real-time kinematic PPP techniques in improving deformation monitoring accuracy. Furthermore, Saracoglu's (2023) study provides valuable insights into how ionospheric variations influence GPS precision over different phases of the solar cycle, adding another dimension to the understanding of GPS performance in deformation monitoring.

The analysis of non-centrality parameters has revealed consistent relationships with session duration, as evidenced in various GPS data processing methodologies. These parameters indicate how well positional changes can be statistically detected. Studies by Meng et al. (2018), Li et al. (2019), Vaclavovic and Nesvadba (2020), Savchyn et al. (2021) and Eren and Hoşbaş (2023) have demonstrated GPS technology's effectiveness in monitoring dynamic displacements, emphasizing the importance of optimized observation periods.

Additionally, Bury et al. (2020) and Kuzikov et al. (2023) highlighted the significance of precise orbit determination in GPS applications, which is inherently connected to extended observation periods.

The devastating Mw 7.2 earthquake that occurred on October 23, 2011, in Van (eastern Türkiye) provides a significant case study for monitoring network sensitivity. This earthquake, followed by an Mw 5.7 aftershock seventeen days later near the town of Edremit, caused extensive damage and has been the subject of numerous geodetic studies. Several researchers have reported co-seismic and post-seismic slip models using geodetic data (Doğan, 2007; Elliott et al., 2013; Fielding et al., 2013; Feng et al., 2014; Doğan et al., 2014; Wang et al., 2021).

This study aims to evaluate the relationship between GPS observing time duration and network sensitivity, particularly focusing on how minimum detectable displacements in a GPS monitoring network vary with station accuracies. For this investigation, we utilized the TUSAGA-AKTIF network in Türkiye, selecting 15 stations over three sequential days in 2011, 2012, and 2013. Our methodology involves:

(I) Analyzing data divided into different session durations (4h, 6h, 12h, and 24h) using Bernese 5.2 GPS software (Dach et al., 2015)
(II) Calculating RMS values for daily repeatability relative to the integrated three-day solution
(III) Computing sensitivity ellipse parameters and drawing these ellipses
(IV) Comparing calculated values across the years 2011, 2012, and 2013

This comprehensive approach allows us to assess the precision agreement between imposed displacements and position variations detected through GPS surveys, while also examining the relationship between observation duration and network sensitivity. The integration of advanced GPS processing techniques, particularly through Bernese software, plays a crucial role in achieving reliable outcomes for varying observation durations.

METHODOLOGY

Sensitivity in deformation monitoring networks is quantified using the non-centrality parameter derived from statistical hypothesis testing. This parameter reflects both the deterministic properties (such as expected deformation patterns) and the stochastic characteristics (such as measurement noise and observational errors) of the network. Consequently, the non-centrality parameter provides a direct estimation of the minimum detectable deformation limit, indicating the smallest deformation that can be identified with a specified confidence level. Mathematically, the objective is to ensure that the estimated non-centrality parameter (λ) for certain probability values (linked to the chosen significance level (α) and test power (β)) exceeds the minimum threshold defined by Baarda's lower bound. If this condition is satisfied, the expected deformation can be considered detectable with the desired statistical confidence. There is a direct relationship between measurement accuracy and the non-centrality parameter. Specifically, higher measurement accuracy results in a larger non-centrality parameter, which corresponds to greater network sensitivity. As a result, the power of the statistical test-reflecting the probability of correctly detecting true deformations-increases.

SENSITIVITY IN GPS DEFORMATION NETWORK

In a GPS network measured in two different periods, coordinate unknowns obtained by adjustment in the same datum are x_N and x_E (Eq. 1) and their matrices of weight coefficients are Q_{EE} and Q_{NN}. Firstly, displacement vector (d**)** is composed (Eq. 3). The matrix of weight coefficients for this vector, Q_{dd}, is constructed assuming there is no correlation between periods (Eq. 3).

$$E = [\ E_1\ E_2\ E_3\ \dots\ \ E_n\ ] \tag{1}$$

$$N = [\ N_1\ N_2\ N_3\ \dots\ \ N_n\ ] \tag{2}$$

$$d = X_E - X_N,\ Q_{dd} =\ Q_{EE} +\ Q_{NN} \tag{3}$$

Secondly, a hypothesis is established to test whether there is a significant change in position between the two periods (Eq. 4):

$$H_0 : E\ (d) = 0$$
$$H_k : E\ (d) \neq 0\ = \Delta \tag{4}$$

If the alternative hypothesis (H_k) is valid, the test is used;

$$T = \frac{d^T {Q_{dd}}^+ d}{{\sigma_d}^2} \sim \chi^2(c, \lambda) \tag{5}$$

This is a non-central χ^2- distribution. c is the rank of cofactor matrix and \sigma_d^2 is the pooled variance, λ is the non-centrality parameter:

$$\lambda = \frac{\Delta^T {Q_{dd}}^+ \Delta}{{\sigma_d}^2} \tag{6}$$

The non-centrality parameter obtained in Eq. (6) is compared with the Baarda (1968)'s lower bound of the non-centrality parameter $\lambda_{0,c}$ (with a certain test power). If $\lambda \geq \lambda_{0,c}$, then the expected displacement vector can be determined as significantly with higher probability than the desired power of the test. Hence, in a GPS deformation network, the result is reached that the changes defined by the Δ vector can occur.

RELATION BETWEEN GPS SESSION DURATION AND SENSITIVITY

The non-centrality parameter is the function of the displacement vector Δ, their cofactor matrix and the pooled variance. Since the matrices of the weight coefficients of the different observation periods are different in comparative periods, the observation times

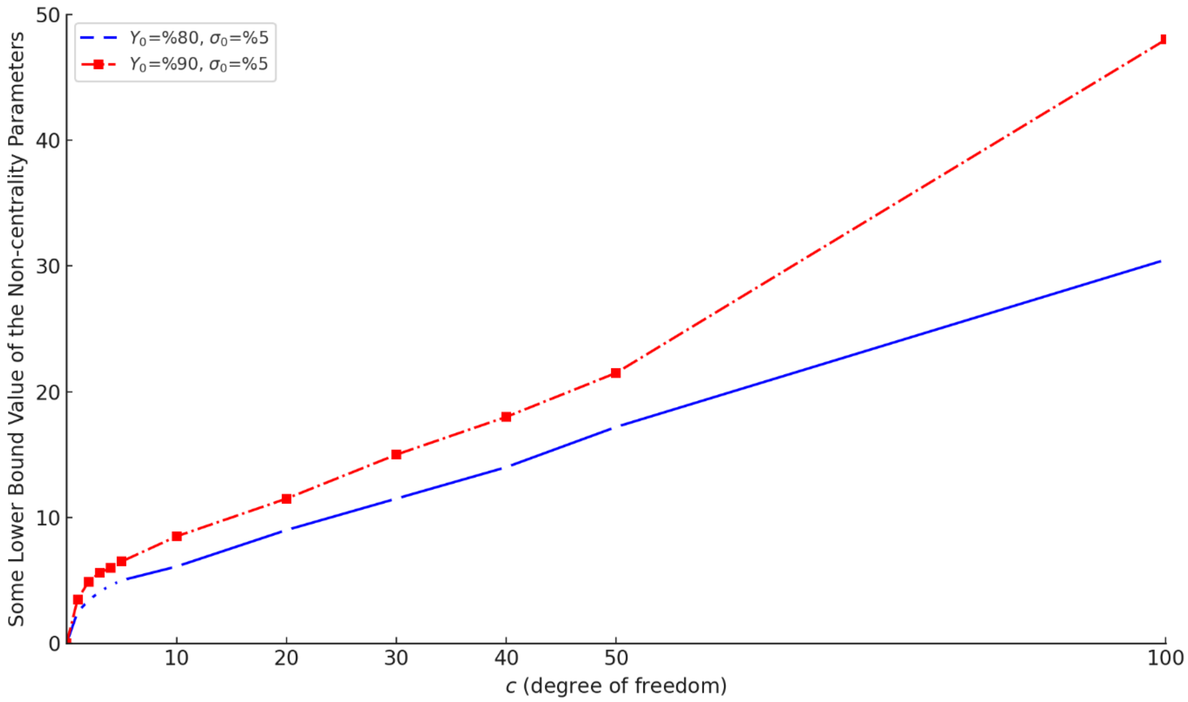

Fig. 1 Some lower bound value of the non-centrality parameters ($\lambda_{0,c}$) for % 80 and % 90 power test (values are taken from Aydin and Demirel, 2005; Aydın et al., 2006 and Aydin, 2011).

affect the matrix of weight coefficients of the displacement vector. So, the sensitivity criterion changes. For t observation session duration, the matrices of the weight coefficients of the coordinate unknowns are Q_{EE} (t) and Q_{NN} (t) respectively for the first and second periods. Δ expected displacement vector is composed in Eq. (7).

Δ= E(d),
(p: number of station) (7)

If the non-centrality parameter for the displacement vector is arranged as a function of the observation period, then it can be expressed using Eq. (8).

$$\lambda(t) = (\Delta^{T} Q_{dd}^{+}(t)\, \Delta)/ \sigma_d^2, \quad Q_{dd}(t) = Q_{EE}(t) + Q_{NN}(t) \qquad (8)$$

MINIMUM DETECTABLE DISPLACEMENTS

The expected displacement vector can be defined as (Eq. 9).

$$\Delta = b\, g \qquad (9)$$

where b is the scale factor and g is the displacement direction vector. Alternatively, the eigen-vectors $\mathbf{\Lambda}_{max}$ and $\mathbf{\Lambda}_{min}$ corresponding to the maximum and minimum eigenvalues of the cofactor matrix Q_{dd} can be used in place of the vector g. In particular, $\mathbf{\Lambda}_{max}$ is associated with the maximum eigen-value λ_{max}. If the displacement vector b $\mathbf{\Lambda}_{max}$, obtained according to Eq. (9), satisfies the inequality $\lambda > \lambda_{0,c}$ and similarly b $\mathbf{\Lambda}_{min}$ satisfies $\lambda > \lambda_{0,c}$ then the values b_a and b_b are determined according to Eqs. (10) and (11), respectively.

$$b_a = \sigma_d \sqrt{\frac{\lambda_{0,c}}{\Lambda_{\max}^{T} Q_{dd}^{+} \Lambda_{\max}}} = \sigma_d \sqrt{\lambda_{0,c} \lambda_{\max}} \qquad (10)$$

$$b_b = \sigma_d \sqrt{\frac{\lambda_{0,c}}{\Lambda_{\min}^{T} Q_{dd}^{+} \Lambda_{\min}}} = \sigma_d \sqrt{\lambda_{0,c} \lambda_{\min}} \qquad (11)$$

The values of b_a and b_b can be determined under the worst case for a deformation network. The displacement vector is defined by "Δ_a = b $\mathbf{\Lambda}_{max}$" and "Δ_b = b $\mathbf{\Lambda}_{min}$". Eq. (12) should be used if it is desired to be found the ratio between the minimum detectable displacement at time t and the minimum detectable displacement at time t_0.

$$\frac{b_t}{b_{t_0}} = \frac{\sigma_d \sqrt{\lambda_{0,c} \lambda_{\max,t}}}{\sigma_d \sqrt{\lambda_{0,c} \lambda_{\max,t_0}}} = \sqrt{\frac{t_0}{t}} \qquad (12)$$

The sensitivity ellipse of a point is drawn from b_a , b_b and θ parameters calculated by using the cofactor matrix of the corresponding point. "b_a" is semi major axis of sensitivity ellipse that is calculated by Eq. (10). "b_b" is semi minor axis of sensitivity ellipse that is calculated by Eq. (11). θ is the orientation of sensitivity ellipse.

NUMERICAL ANALYSIS

GPS DATA AND ANALYSIS

In this study, a GPS deformation monitoring network was established using the TUSAGA-AKTIF

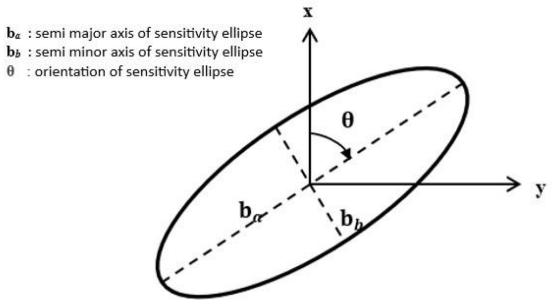

Fig. 2 Sensitivity ellipse and its parameters.

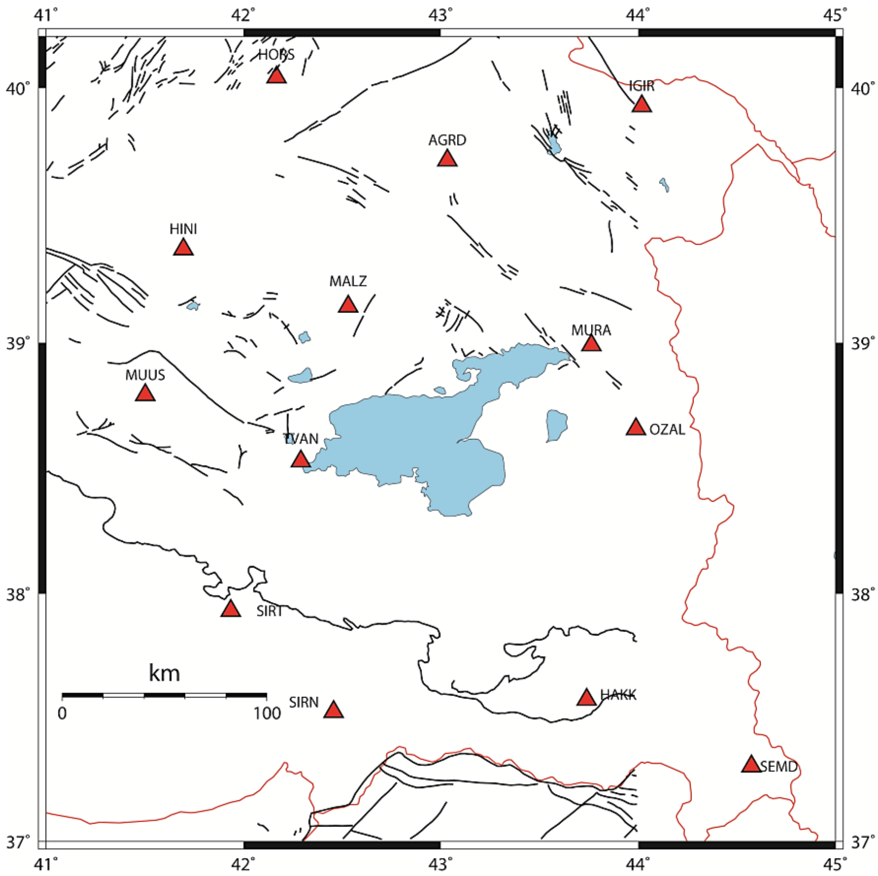

Fig. 3 Spatial distribution of the GPS stations in the Lake Van region, eastern Türkiye. The map highlights significant fault zones and station placements, which are crucial for detecting crustal deformations and analyzing the geodetic response to the 2011 Van earthquake.

network to monitor and model deformation processes, as well as to determine network sensitivity and minimum detectable displacements. The GPS data sets were collected from TUSAGA-AKTIF stations over three successive days in 2011, 2012, and 2013 (Fig. 3). The GPS observations were conducted between Days 292–294 in 2011, Days 256–258 in 2012, and Days 263–265 in 2013, in order to have consistency in temporal data distribution for the comparison. The TUSAGA-AKTIF network was selected due to its dense station distribution and high positional accuracy, making it suitable for regional deformation monitoring studies.

The collected data consists of daily observation files recorded at a 30-second sampling interval, ensuring adequate temporal resolution for deformation analysis. All data were processed using a satellite elevation cut-off angle of 10°, which is a standard threshold to minimize multipath effects and reduce signal noise from low-elevation satellites.

To investigate how observing session duration affects the sensitivity of the GPS network, the data were divided into four categories of observing session length: 4 hours, 6 hours, 12 hours, and 24 hours (Table 1). This segmentation allows for the assessment of how shorter observation periods affect

Table 1 Sessions designations.

Session Length (h)	Session Timing						Sessions
	a	b	c	D	e	f	
4	00-04	04-08	08-12	12-16	16-20	20-24	6
6	00-06	06-12	12-18	18-24			4
12	00-12	12-24					2
24	00-24						1

the detection capability of potential deformations, which is crucial for optimizing network design in scenarios where continuous long-term observations may not be feasible. Additionally, the details of GPS observations, including station characteristics and equipment configurations, offering a comprehensive overview of the data sources used in this study.

The GPS data were processed using the BERNESE V5.2 software (Dach et al., 2015), ensuring high positional accuracy through the utilization of IGS final precise ephemeris and earth rotation parameters. The dataset comprised 24-hour sessions for continuously operating stations and 8–10-hour sessions for campaign sites, with a sampling interval of 30 seconds. To maintain data quality, cycle slip detection and correction were applied to L1 and L2 phase measurements at both triple- and double-difference levels (Eckl et al., 2001). The ionosphere-free linear combination (L3) was employed for the final baseline solution to mitigate first-order ionospheric effects, while integer ambiguity resolution for L1/L2 phase data was performed using the Quasi-Iono Free (QIF) strategy (Dach et al., 2015). A minimum elevation cut-off angle of 10° was set to minimize multipath interference and ensure a reliable signal-to-noise ratio (Hager et al., 1991). For tropospheric delay modeling, the Saastamoinen (1972)´s model was applied under a standard atmospheric assumption, with tropospheric delays mapped using the Vienna Mapping Function (VMF1) (Böhm et al., 2006). Tropospheric zenith delays were estimated at two-hour intervals to account for temporal atmospheric variations. Furthermore, corrections for antenna phase center variations (PCV) were implemented following the IGS absolute phase center model (Schmid et al., 2007). The coordinate solutions were referenced to the ITRF2008 framework (Altamimi et al., 2011), with the HORS station fixed as a stable reference point, as it is located outside major seismically active fault zones. Additionally, earth orientation parameters, polar tide corrections, and ocean tide loading effects were accounted for using IERS2010 conventions (Petit and Luzum, 2010) and the FES2004 model (Lyard et al., 2006), respectively. The use of IGS final orbit products further ensured the precise determination of satellite positions (Erkoç and Doğan, 2023). The quality of daily solutions was rigorously evaluated by computing repeatability metrics, specifically root mean square (RMS) values, relative to a three-day integrated solution. This allowed for a robust assessment of temporal stability and accuracy across all sessions.

Figure 4 illustrates the RMS values for the east and north components for all stations within the 2011 dataset, analyzed across four different observation durations: 4-hour, 6-hour, 12-hour, and 24-hour sessions. The results demonstrate a clear trend where RMS values decrease with longer observation periods, underscoring the positive correlation between session length and positional precision. In particular, the 24-hour sessions yielded RMS values below 2 mm in the horizontal components at most stations, indicative of high measurement accuracy. However, an exception was observed at the SIRN station during the 4-hour session, where the east-component RMS exceeded 8 mm. This anomaly suggests the influence of localized environmental factors, potential multipath interference, or reduced signal quality during shorter sessions. Conversely, stations such as AGRD, HINI, and MALZ consistently exhibited lower RMS values across all observation durations, reflecting optimal site conditions and advantageous network geometry.

A comparative analysis of the four observation durations, as depicted in Figure 4, reveals a substantial improvement in daily solution repeatability with increased session length. As an example, Figure 4 presents the RMS values for the year 2011. Instead of including multiple images, we provide a representative case of RMS values for all stations. Additionally, Table 2 highlights the RMS values of a single station (HINI) for 2011, 2012, and 2013 to illustrate the temporal consistency of the results across multiple years. Shorter sessions (4h and 6h) displayed greater variability in RMS values, particularly at stations situated near tectonically active regions, whereas 12-hour and 24-hour sessions produced more consistent and lower RMS distributions. This finding reinforces the necessity of extended observation durations to achieve reliable deformation monitoring.

As an example, Figure 4 presents the RMS values for the year 2011. Instead of including multiple images, we provide a representative case of RMS values for all stations. Additionally, Table 2 highlights the RMS values of a single station (HINI) for 2011, 2012, and 2013 to illustrate the temporal consistency of the results across multiple years.

To complement the RMS analysis presented in Figure 4, a detailed deformation analysis was conducted to evaluate positional changes between consecutive observation periods (2011–2012 and 2012–2013). Table 3 summarizes the coordinate differences in the north-south and east-west directions, along with the deformation status for each station.

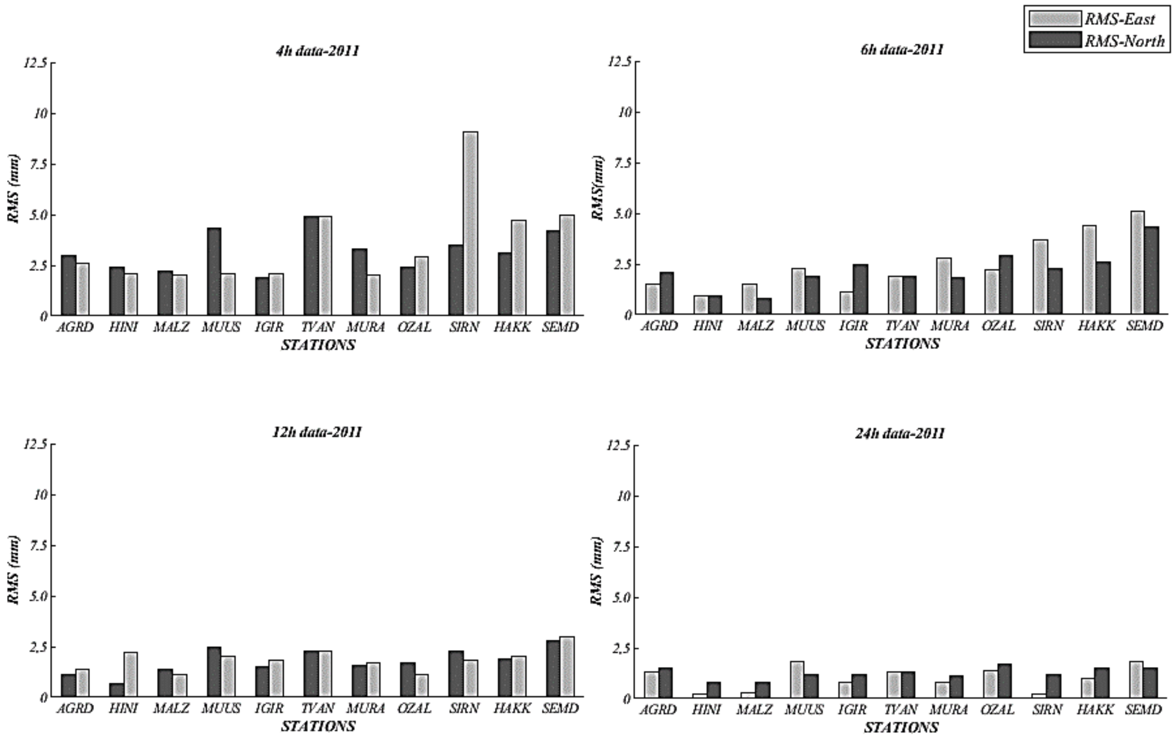

Fig. 4 RMS values for daily solution repeatability in the east and north directions across selected TUSAGA-AKTIF stations for the year 2011, based on 4-hour, 6-hour, 12-hour, and 24-hour observation sessions.

Table 2 RMS Values for HINI Station (2011-2013).

Year	Coordinate	4h-RMS (mm)	6h- RMS (mm)	12h- RMS (mm)	24h- RMS (mm)
2011	North	2.5	2.0	1.8	1.5
	East	3.0	2.5	2.0	1.8
2012	North	2.8	2.4	2.0	1.7
	East	3.2	2.7	2.2	1.8
2013	North	3.0	2.7	2.2	1.7
	East	3.1	2.9	2.3	2.0

Table 3 Deformation Analysis Between Observation Periods (2011–2013).

	Coordinate Differences					
	2011–2012			2012–2013		
Station	North (mm)	East (mm)	χ^2 Value	North (mm)	East (mm)	χ^2 Value
AGRD	-28.5	6.4	32.7	-6.8	-3.6	7.4
HAKK	28.0	-10.2	115.5	-9.1	-0.1	10.9
HINI	9.4	-10.8	60.2	4.0	-6.2	7.7
IGIR	-2.6	-3.0	5.1	-8.8	-0.9	6.2
MALZ	-8.9	2.7	6.3	0.9	0.9	7.2
MURA	-68.5	-7.8	199.4	1.3	-1.3	6.9
MUUS	12.1	-13.6	50.7	4.0	-6.8	6.8
OZAL	38.7	-5.2	364.1	10.3	-6.3	23.7
SEMD	33.3	-7.7	156.8	11.1	-1.1	15.58
SIRN	16.5	-9.8	36.9	5.5	-3.3	5.26
SIRT	15.8	-9.6	37.8	12.4	-14.2	71.4
TVAN	14.8	-16.5	79.7	3.3	-13.7	36.8

A comprehensive deformation analysis was conducted to assess the positional variations of selected GNSS stations over two consecutive periods: 2011–2012 and 2012–2013. The results, presented in Table 3, reveal that the majority of stations exhibited consistent kinematic trends across both periods, indicating sustained geodynamic activity in the region. Notably, stations such as AGRD, HAKK, HINI, MURA, MUUS, OZAL, SEMD, SIRN, SIRT, and TVAN demonstrated significant displacements in both the north-south and east-west directions, underscoring active crustal deformation. Among these, OZAL recorded the highest northward displacement (38.7 mm) during the 2011–2012 period, with continued deformation in the subsequent year.

The observed deformations in the 2011–2012 period can be primarily attributed to post-seismic processes triggered by the 2011 Van earthquake. However, the 2012–2013 results indicate that ongoing aftershocks and the region's persistent tectonic activity continued to influence ground displacements. The sustained deformation observed at several stations, particularly SEMD, SIRT, and TVAN, suggests that post-seismic relaxation and secondary fault movements played a significant role in the regional kinematics beyond the immediate co-seismic effects. Furthermore, MUUS and SEMD, which were previously underemphasized, exhibited persistent deformation trends, reinforcing the evidence for ongoing tectonic processes. In contrast, IGIR and MALZ remained relatively stable across both periods, suggesting localized tectonic quiescence. To statistically evaluate the significance of the observed displacements, a chi-square (χ^2) test was applied to each station's positional variations. Given the degrees of freedom in this analysis, a critical χ^2 threshold of 7.81 was adopted as the significance limit. The results indicate that stations such as OZAL (χ^2 = 364.1), MURA (χ^2 = 199.4), and SEMD (χ^2 = 156.8) exhibit highly significant deformation patterns, whereas IGIR (χ^2 = 5.1) and MALZ (χ^2 = 6.3) remain below the significance threshold, supporting the inference of their relative stability.

These findings provide critical insights into the post-seismic deformation patterns following the 2011 Van earthquake. The continuation of significant displacements during the 2012–2013 period highlights the influence of aftershocks and regional tectonic activity on crustal dynamics. This underscores the necessity of long-term GNSS monitoring to fully capture the temporal evolution of deformation and enhance seismic hazard assessments in the region.

SENSITIVITY ANALYSIS AND RESULTS

After calculating the displacement vector (d) and the corresponding weight coefficient matrix (Q_{dd}), a hypothesis test was conducted to determine whether there was a statistically significant positional change between the two observation periods. This hypothesis follows a non-central χ^2 distribution, which allows for the calculation of the non-centrality parameter (λ). The calculated λ values were then compared against the minimum threshold defined by Baarda (1968)'s non-centrality parameter ($\lambda_{0,c}$) to assess the detectability of positional changes.

Subsequently, Eqs. (10) and (11) were employed to compute the semi-major (b_a) and semi-minor (b_a) axes of the sensitivity ellipses for the years 2011, 2012, and 2013. These parameters provide insights into the directional sensitivity and accuracy of the GPS network, highlighting the axes along which the network is most responsive to deformation. The sensitivity ellipses were drawn for different observation session durations (4h, 6h, 12h, and 24h) corresponding to the 2011 dataset. Additionally, co-seismic displacement vectors were superimposed on the ellipses to visually represent the magnitude and direction of the observed displacements (Figs. 5, 6, 7, and 8). The size and orientation of these ellipses indicate the minimum detectable displacement thresholds, with longer observation durations generally yielding smaller ellipses, thus representing higher sensitivity. The analysis revealed that 24-hour sessions provided the highest sensitivity, with the smallest ellipse dimensions across most stations. In contrast, shorter sessions (4h and 6h) resulted in larger ellipses, reflecting lower sensitivity and higher detection limits. Moreover, stations located in close proximity to active fault zones exhibited larger displacement vectors, consistent with the expected co-seismic deformation patterns following the 2011 Van earthquake. The final step in the sensitivity analysis involved determining the ratio of $\frac{b_t}{b_{t_0}}$, where b_t represents the sensitivity parameter at a given session duration t and b_{t_0} corresponds to the reference session duration (t_0). The theoretical relationship between these parameters is given by Eq. (12) (This equation was also utilized to calculate $\frac{b_t}{b_{t_0}}$ ratios for the years 2011**,** 2012**,** and 2013**).** The results provide insights into how observation duration impacts the sensitivity of the GPS network. As an example, Figure 9 shows the calculated $\frac{b_t}{b_{t_0}}$ values for 2011 across selected GPS stations. The graph illustrates the relationship between the observation session durations (6h, 12h, and 24h) relative to the 4h reference session**.**

Figure 9 reveals a general trend where the ratio $\frac{b_t}{b_{t_0}}$ decreases as the observation duration increases, indicating higher sensitivity for longer sessions. Specifically:

- The 6h/4h ratio shows relatively high consistency across stations, with values ranging between 0.75 and 0.82, suggesting moderate sensitivity improvements.
- The 12h/4h ratio decreases further, reflecting enhanced sensitivity with a value around 0.58–0.60.

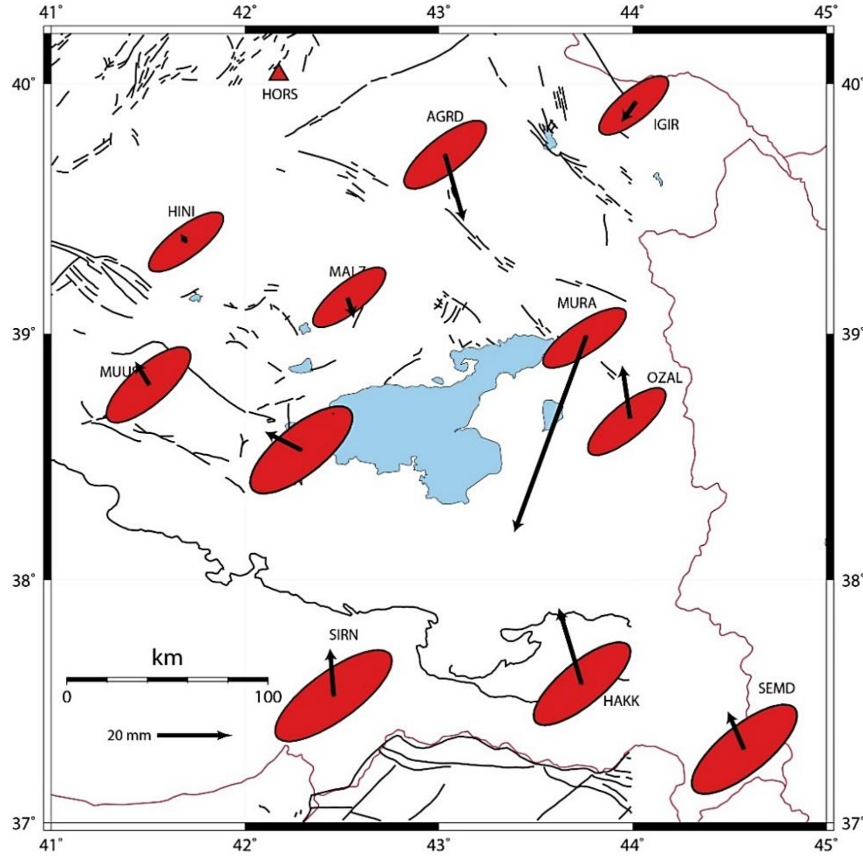

Fig. 5 Sensitivity ellipses of 2011 from 4h data.

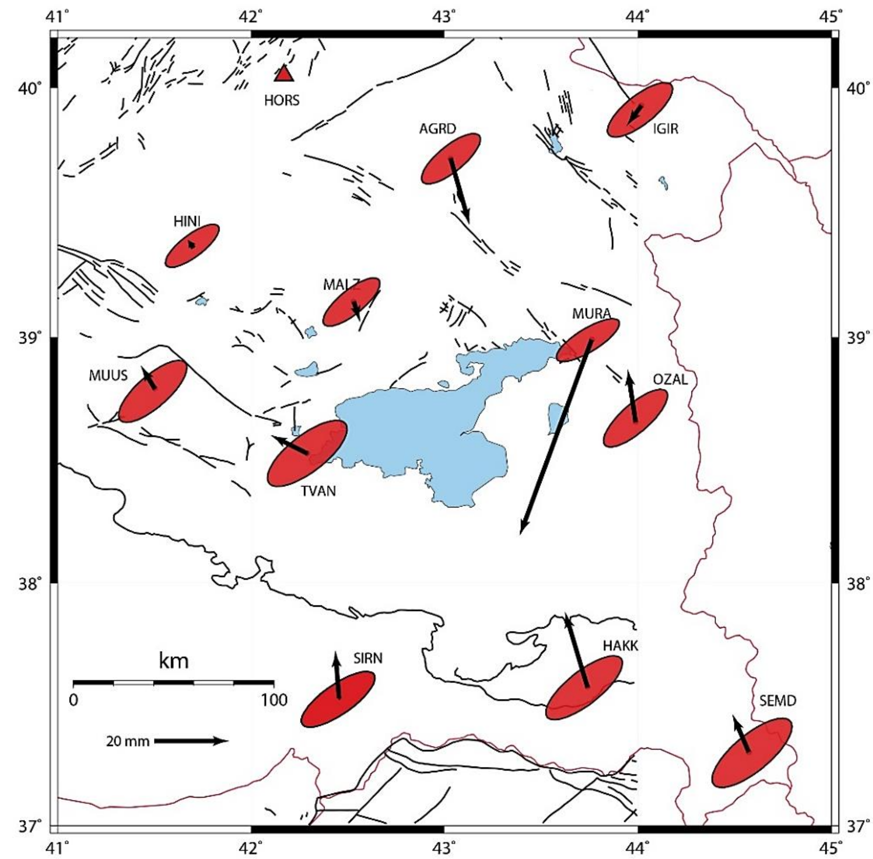

Fig. 6 Sensitivity ellipses of 2011 from 6h data.

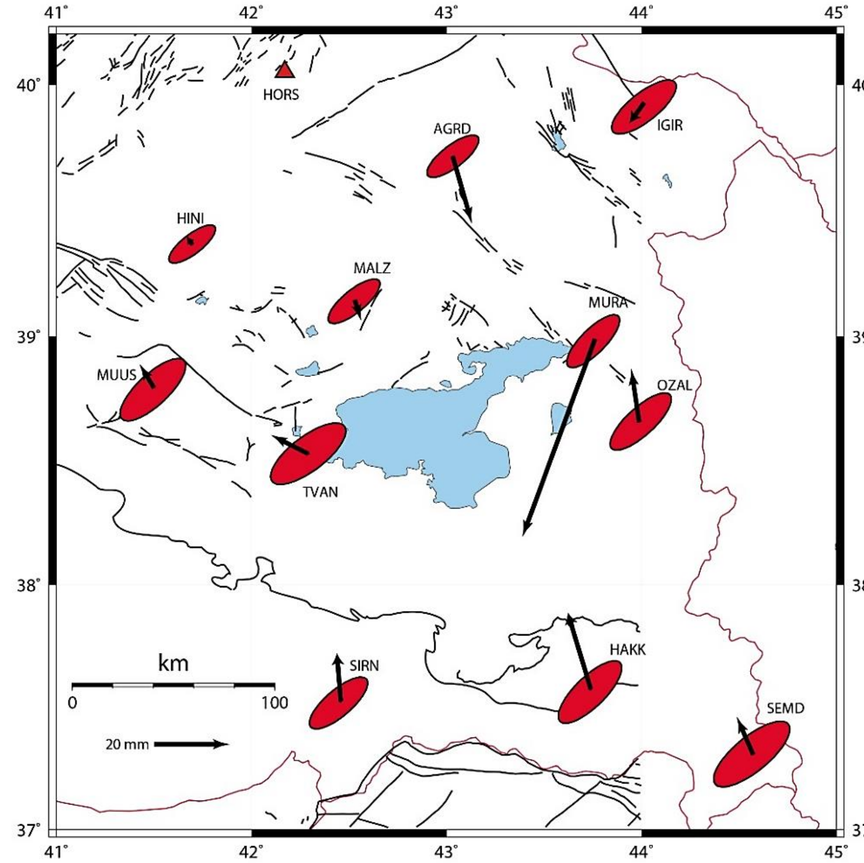

Fig. 7 Sensitivity ellipses of 2011 from 12h data.

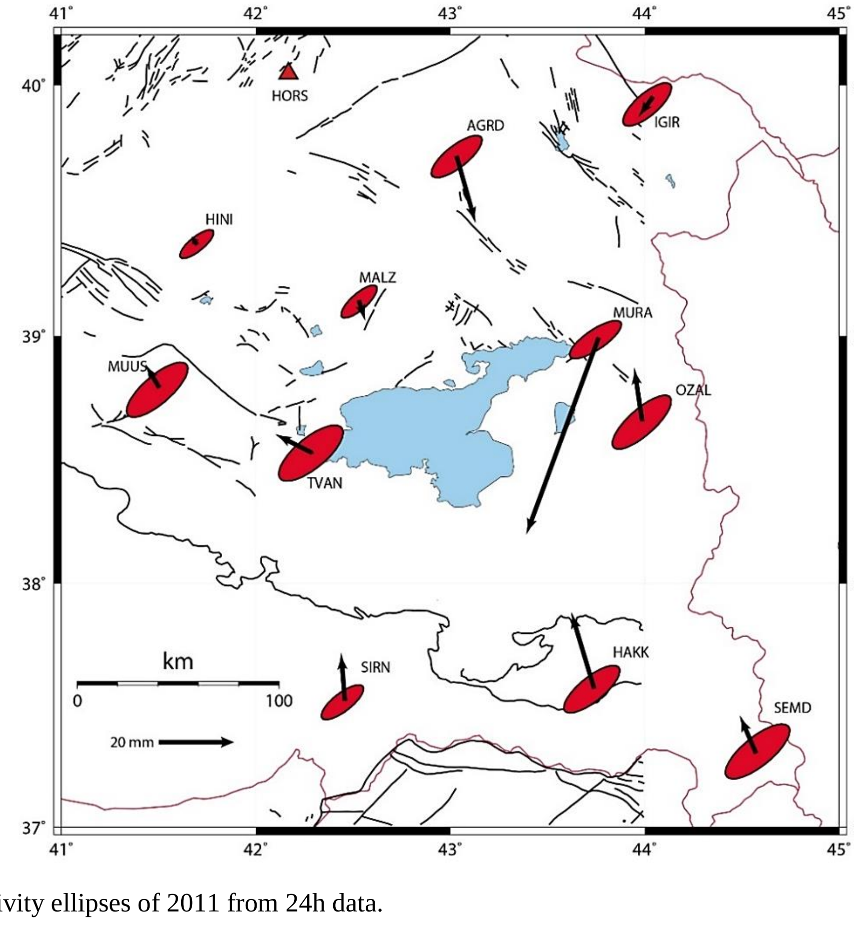

Fig. 8 Sensitivity ellipses of 2011 from 24h data.

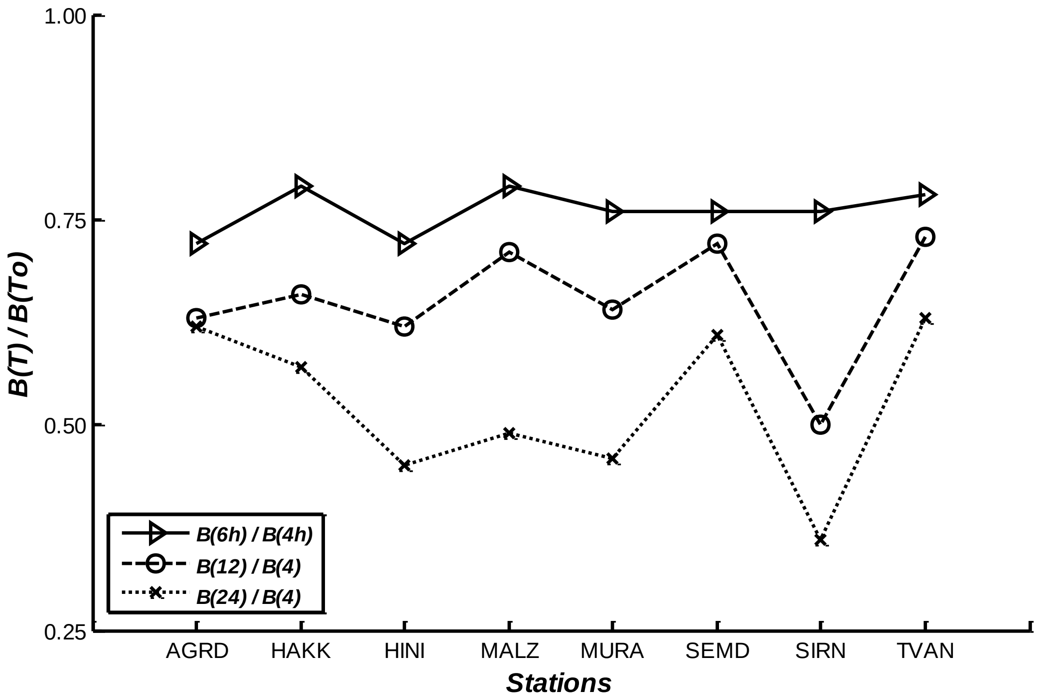

Fig. 9 Calculated $\frac{b_t}{b_{t_0}}$ values-2011.

Table 4 Comparison of $\frac{b_t}{b_{t_0}}$ and $\sqrt{\frac{t_0}{t}}$.

Year	b(t)/b(t_0)		
	(6/4)	(12/4)	(24/4)
2011	**0.76**	**0.60**	**0.49**
2012	**0.80**	**0.59**	**0.42**
2013	**0.81**	**0.58**	**0.41**
Com. Value		$\sqrt{(t_0/t)}$	
	0.82	**0.58**	**0.41**

- The 24h/4h ratio exhibits the lowest values (0.41–0.49), indicating the highest sensitivity due to prolonged observation time.

The calculated ratios were subsequently compared with the theoretical values derived from $\sqrt{\frac{t_0}{t}}$**,** as presented in Table 4**.**

Table 4 presents a direct comparison between the calculated ratios and theoretical values. The results indicate:

- For the 6h/4h ratio, calculated values (0.76–0.81) were slightly lower than the theoretical value (0.82), likely due to measurement noise and station-specific observational conditions.
- For the 12h/4h ratio, the calculated values (0.58–0.60) aligned closely with the theoretical value (0.58), confirming the model's validity.
- The 24h/4h ratio showed perfect agreement (0.41) across all years, matching the theoretical expectation exactly, which suggests stable observational conditions and high positional repeatability for extended sessions.

These findings demonstrate that longer GPS observation sessions significantly enhance the sensitivity of the monitoring network by reducing the minimum detectable deformation limits.

DISCUSSION

This study has provided a comprehensive examination of the relationship between GPS observation duration and deformation network sensitivity, emphasizing the detection of minimum displacement thresholds. The findings confirm that longer observation sessions yield higher network sensitivity, with 24-hour sessions producing the smallest sensitivity ellipses and lower RMS values. The inverse correlation between observation duration and sensitivity ellipse size highlights the critical role of session length in optimizing GPS deformation networks, particularly in tectonically active regions. Notably, while 12-hour sessions demonstrated a sensitivity level comparable to 24-hour sessions, shorter durations such as 4-hour and 6-hour sessions showed decreased sensitivity, underscoring the trade-off between observation time and network performance.

When compared with existing literature, the results align well with previous research. Studies by Even-Tzur (2002) and Stoper (2001) similarly identified observation duration as a crucial factor influencing network accuracy. Additionally, the close alignment between calculated ratios and theoretical values derived from Baarda’s (1968) non-centrality parameter further validates the proposed methodology. This study adds unique value by applying the model to TUSAGA-AKTIF stations in the Lake Van region, offering empirical evidence of its effectiveness in a complex tectonic setting. The consistency between observed co-seismic displacement vectors and calculated sensitivity ellipses further reinforces the method's robustness.

The practical implications of these findings are significant. The results suggest that 12-hour observation sessions could provide an effective balance between operational efficiency and sensitivity, especially where continuous long-term data collection is challenging. Moreover, stations situated closer to active fault zones exhibited larger displacement vectors, emphasizing the need for denser station networks in such areas. These insights align with recommendations from previous studies that highlight the importance of strategic station placement for accurate deformation monitoring.

Despite these contributions, the study has certain limitations. The focus on data from 2011 to 2013 may limit the generalizability of the results to other regions or time frames. Additionally, while atmospheric effects were minimized using standard correction models, residual influences, particularly during shorter sessions, may affect sensitivity estimates. Future research should address these limitations by exploring real-time GPS processing techniques, integrating multi-GPS constellations, and employing machine learning algorithms to further refine sensitivity models. Expanding the geographical scope of the analysis to include various tectonic environments would also help validate the general applicability of the proposed methodology.

CONCLUSION

In this study, the influence of observation session duration on deformation monitoring network sensitivity in the Van region, Türkiye, was analyzed. The results indicated a clear inverse relationship between observation duration and sensitivity ellipse size and that 24-hour observation sessions provide optimal sensitivity with a cost-saving alternative of 12-hour observation sessions without significant sensitivity loss. The strong correlation between theoretical predictions and empirical observations confirmed the suitability of the non-centrality parameter-based model used. Moreover, the effect of the distance between stations and active fault zones on displacement detection emphasizes the importance of strategic station placement in network design.

Generally, this research provides practical suggestions for real-time optimization of GPS deformation networks with a balance between high sensitivity and operational efficiency. Future work might involve real-time data processing, multi-GNSS integration, and machine learning strategies to further optimize dynamic deformation monitoring.

ACKNOWLEDGEMENTS

The General Directory of Land Registry and Cadastre and the General Directorate of Mapping provided TUSAGA-AKTIF stations RINEX files. ChatGPT was utilized for English language checks/English editing in this paper. We used GMT for the figures (Wessel et al., 2013).

REFERENCES

Alizadeh Khameneh, M.A., Eshagh, M. and Sjöberg L.E.: 2015, Optimisation of Lilla Ezet Landslide GPS monitoring network. J. Geod. Sci., 5, 1, 57–66. DOI: 10.1515/jogs-2015-0005

Altamimi, Z., Collilieux, X. and Métivier, L.: 2011, ITRF2008: An improved solution of the International Terrestrial Reference Frame. J. Geod., 85, 8, 457–473. DOI: 10.1007/s00190-011-0444-4

Aydin, C.: 2011, Power of global test in deformation analysis. J. Surv. Eng., 138, 2, 51–56. DOI: 10.1061/(asce)su.1943-5428.0000064

Aydin, C. and Demirel, H.: 2005, Computation of Baarda's lower bound of the non-centrality parameter. J. Geod., 78, 7, 437–441. DOI: 10.1007/s00190-004-0406-1

Aydın, C., Doğan, U. and Demirel, H.: 2006, Relation between session-duration and sensitivity of GPS monitoring networks. Harit. derg., 73, 135, 42–51, (in Turkish).

Baarda, W.: 1968, A testing procedure for use in geodetic networks. Publications on Geodesy, new series, 2, 5. Netherlands Geodetic Commission, Delft, Netherlands.

Betti, B., Biagi, L., Crespi, M. and Riguzzi, F.: 1999, GPS sensitivity analysis applied to non-permanent deformation control networks, J. Geod., 73, 158–167. DOI: 10.1007/s001900050231

Böhm, J., Werl, B. and Schuh, H.: 2006, Troposphere mapping functions for GPS and very long baseline interferometry from European Centre for Medium-Range Weather Forecasts operational analysis data. J. Geophys. Res., Solid Earth, 111, B02406. DOI: 10.1029/2005JB003629

Bury, G., Sośnica, K., Zajdel, R., Strugarek, D. and Hugentobler, U.: 2020, Determination of precise Galileo orbits using combined GNSS and SLR observations. GPS Solut., 25, 1. DOI: 10.1007/s10291-020-01045-3

Dach, R., Lutz, S., Walser, P. and Fridez, P.: 2015, Bernese GNSS Software Version 5.2 User Manual. Astronomical Institute, University of Bern, Bern Open Publishing. DOI: 10.7892/boris.72297

Doğan, U.: 2007, Accuracy analysis of relative positions of permanent GPS stations in the Marmara Region, Turkey. Surv. Rev., 39, 304, 156–165. DOI: 10.1179/003962607x165113

Dogan, U., Demir, D.Ö., Çakir, Z., Ergintav, S., Ozener, H., Akoğlu, A.M., Nalbant, S.S. and Reilinger, R: 2014, Postseismic deformation following the Mw 7.2, 23 October 2011 Van earthquake (Turkey): evidence for aseismic fault reactivation. Geophys. Res. Lett., 41, 2334–2341. DOI: 10.1002/2014GL059291

Eckl, M.C., Snay, R.A., Soler, T., Cline, M.W. and Mader, G.L.: 2001, Accuracy of GPS derived relative positions as a function of interstation. J. Geod., 75, 633–640. DOI: 10.1007/s001900100204

Elliott, J., Copley, A., Holley, R., Scharer, K. and Parsons, B.; 2013, The 2011 Mw 7.1 Van (eastern Turkey) earthquake. J. Geophys. Res., Solid Earth, 118, 1619–1637. DOI: 10.1002/jgrb.50117

Eren, M. and Hoşbaş, R.G.: 2023, Testing the performance of the video camera to monitor the vertical movements of the structure via a specially designed steel beam apparatus. Meas. Sci. Rev., 23, 1, 32–39. DOI: 10.2478/msr-2023-0004

Erkoç, M.H. and Doğan, U.: 2023, Datum definition for geodetic vertical velocity field derived from GNSS observations: a case study in western and southern Turkey. Boll Geofis Teor Appl., 63, 1, 135–148. DOI: 10.4430/bgo00412

Even-Tzur, G.: 1999, Sensitivity design for monitoring deformation networks. Boll. Geod. Sci. Aff., 4, 313–324.

Even-Tzur, G: 2002, GPS vector configuration design for monitoring deformation networks. J. Geod., 76, 8, 455–461. DOI: 10.1007/s00190-002-0274-5

Feng, W., Li, Z., Hoey, T., Zhang, Y., Wang, R., Samsonov, S., Li, Y. and Xu, Z: 2014, Patterns and mechanisms of coseismic and postseismic slips of the 2011 MW7.1 Van (Turkey) earthquake revealed by multi-platform synthetic aperture radar interferometry. Tectonophysics, 632, 188–198. DOI: 10.1016/j.tecto.2014.06.011

Fielding, E.J., Lundgren, P.R., Taymaz, T., Yolsal-Çevikbilen, S. and Owen, S.E.: 2013, Fault-slip source models for the 2011 M 7.1 Van earthquake in Turkey from SAR interferometry, pixel offset tracking, GPS, and seismic waveform analysis. Seismol. Res. Lett., 84, 579–593. DOI: 10.1785/0220120164

Forootan, E., Farzaneh, S. and Naderi, K.: 2021, Analyzing GNSS measurements to detect and predict bridge movements using the Kalman filter (KF) and neural network (NN) techniques. Geomatics, 1, 1, 65–80. DOI:10.3390/geomatics1010006

Hager, B.H., King, R.W. and Murray, M.H.: 1991, Measurements of crustal deformation using the Global Positioning System. Annu. Rev. Earth Planet. Sci., 19, 351–382. DOI: 10.1146/annurev.ea.19.050191.002031

Koch, K.R.: 1988, Bayesian statistics for variance components with informative and noninformative priors. Manuscr. Geod., 13, 8, 370–373. DOI: 10.1007/BF03655190

Kuang, S.: 1991, Optimization and design of deformation monitoring schemes. Ph.D. Dissertation, Department of Surveying Engineering, Technical Report No. 157, University of New Brunswick, Canada.

Kuzikov, S., Kenigsberg, D., Salamatina, Y. and Prokhorov, O.: 2023, Comparison of methods for computing highly accurate daily GNSS position. Civ. Eng. J., 9, 2, 305–318. DOI:10.28991/cej-2023-09-02-04

Li, Y., Xu, C., Chen, C., Yin, H., Yi, L. and He, X.: 2019, Adaptive denoising approach for high-rate GNSS seismic waveform preservation: application to the 2010 El Mayor-Cucapah earthquake and 2012 Brawley seismic swarm. IEEE Access, 7, 173166–173184. DOI: 10.1109/access.2019.2956780

Lyard, F., Lefevre, F. and Letellier, T.: 2006, Modelling the global ocean tides: modern insights from FES2004. Ocean Dyn., 56, 394–415. DOI: 10.1007/s10236-006-0086-x

Martin, A., Anquela, A.B., Dimas-Pagés, A. and Cos-Gayón, F.: 2015, Validation of performance of real-time kinematic PPP. A possible tool for deformation monitoring. Measurement, 69, 95–108. DOI: 10.1016/j.measurement.2015.03.026

Meng, X., Xi, R. and Xie, Y.: 2018, Dynamic characteristic of the Forth Road Bridge estimated with GeoSHM. J. Glob. Position. Syst., 16, 1. DOI: 10.1186/s41445-018-0014-7

Petit, G. and Luzum, B.E. (eds): 2010, IERS Convention International Earth Rotation and Reference Systems Service (IERS). IERS Technical Note No. 36. Verlag des Bundesamts fur Kartographie und Geodasie, Frankfurt am Main, Germany, 179 pp.

Saracoglu, A.: 2024, Causal insights into GPS precision variability: an investigation into the ionospheric impact on GPS measurements throughout the solar cycle. Bull. Geophys. Oceanogr., 65, 1, 77–86. DOI: 10.4430/bgo00438

Saastamoinen, J.: 1972, Atmospheric correction for the troposphere and stratosphere in radio ranging of satellites. Artif. Satell. Geod., 15, 247–25. DOI: 10.1029/GM015p0247

Savchyn, I., Tretyak, K., Hlotov, V., Shylo, Y., Bubniak, I., Golubinka, I. and Nikulishyn, V.: 2021, Recent local geodynamic processes in the Penola Strait – Lemaire Channel fault area (West Antarctica). Acta Geodyn. Geomater., 18, 2, 202, 253–265. DOI: 10.13168/AGG.2021.0018

Schmid, R., Steigenberger, P., Gendt, G., Ge, M. and Rothacher, M.: 2007, Generation of a consistent absolute phase-center correction model for GPS receiver and satellite antennas. J. Geod., 81, 12, 781–798. DOI: 10.1007/s00190-007-0148-y

Stoper, B.: 2001, Second order design of horizontal GPS Net. Surv. Rev., 36, 279, 44–53. DOI: 10.1179/sre.2001.36.279.44

Vaclavovic, P. and Nesvadba, O.: 2020, Comparison and assessment of float, fixed, and smoothed precise point positioning. Acta Geodyn. Geomater., 17, 3(199), 329–340. DOI: 10.13168/AGG.2020.0024

Wang, X., Zhao, Q., Xi, R., Lin, M., Li, G. and Li, L.: 2021, Review of bridge structural health monitoring based on GNSS: from displacement monitoring to dynamic characteristic identification. IEEE Access, 9, 80043–80065. DOI: 10.1109/access.2021.3083749

Wessel, P., Smith, W.H.F., Scharroo, R., Luis, J. and Wobbe, F.: 2013, GMT Generic mapping tools: Improved version released. EOS, Trans. AGU, 94, 409–410. DOI: 10.1002/2013EO450001

Xu, P. and Grafarend, E.: 1995, A multi-objective second-order optimal design for deforming networks. Geophys. J. Int., 120, 577–589. DOI: 10.1111/j.1365-246X.1995.tb01840.x